RESEARCH ARTICLE

Recent wetting trend in China from 1982 to 2016 and the impacts of extreme El Niño events

Hao Yan[1,2] ⓘ | Shao-Qiang Wang[3,4] | Jun-Bang Wang[3] | An-Hong Guo[1] |
Zai-Chun Zhu[5] | Ranga B. Myneni[6] | Herman H. Shugart[2]

[1]National Meteorological Center, China Meteorological Administration, Beijing, China

[2]Environmental Sciences Department, University of Virginia, Charlottesville, Virginia

[3]Key Lab of Ecosystem Network Observation and Modelling, Institute of Geographic Sciences and Natural Resources Research, Chinese Academy of Sciences, Beijing, China

[4]College of Resources and Environment, University of Chinese Academy of Sciences, Beijing, China

[5]School of Urban Planning and Design, Shenzhen Graduate School, Peking University, Shenzhen, China

[6]Department of Earth and Environment, Boston University, Boston, Massachusetts

Correspondence
Hao Yan, National Meteorological Center, Zhongguancun South Street #46, Haidian district, 100081 Beijing, China.
Email: yanhaon@hotmail.com

Funding information
National Key Research and Development Program of China, Grant/Award Number: 2017YFC1502402; National Natural Science Foundation of China, Grant/Award Number: 41571327

Abstract

Climate warming generally is expected to increase drought, but arguments about China's past drought trends persist. $PDSI_{ARTS}$, a revised self-calibrating Palmer Drought Severity Index, was computed for China over 1982–2016 using satellite leaf-area indices combined with monthly climate data interpolated from 2000 high-density stations. Drought climatology was analysed against climate factors. The results show that temperature has increased at a rate of $0.38°C$ per decade ($p < .001$) in China in the past 35 years (1982–2016). However, over the same interval, China and the northern China region became wetter. $PDSI_{ARTS}$ increased at a rate of $0.03 \, yr^{-1}$ ($p < .001$) across China during 1982–2016. The analogous increase of $PDSI_{ARTS}$ in northern China was $0.05 \, yr^{-1}$ ($p < .001$). In China, the 5-year interval from 2012 to 2016 was the wettest 5 years in the 35-year interval. This arises from the coupled effects of decreased potential evaporation (E_p) and increased precipitation (P_r). The implication is that temperature increase does not necessarily indicate increased drought. A potential complication is that the 2015/16 El Niño event induced the highest P_r in southern China for 1982–2016, and northern China still had plentiful P_r in 2015/16, which further contributed to the wettest 2-years (2015/16) during the past 35 years in the whole of China. This study highlights the joint impacts of P_r and E_p on the dry/wet changes and the possibility of extremely wet events in the warming future.

KEYWORDS
drought, El Niño event, extreme wet era, PDSI, wetter climate

1 | INTRODUCTION

Under typical monsoon climate, China frequently features drought/flood events (Zou and Zhai, 2004; Yan *et al.*, 2016; Sun *et al.*, 2017). Drought, as a critical natural hazard, often causes vegetation degradation and crop yield decrease in China. For example, the drought occurring in 2000 and 2001 has been regarded as the most serious drought during the 1982–2011 interval (Yan *et al.*, 2016). It caused a sharp decrease of spring vegetation coverage and contributed to frequent spring dust storms and heavy air pollution over northern China (Zou and Zhai, 2004).

Atmosphere and land have complex interactions, which produce large uncertainties and other difficulties in drought monitoring. Numerous drought-indices including climatic drought-indices and remote-sensing-derived

drought-indices have been developed to detect and monitor meteorological droughts (Palmer, 1965; Yan *et al.*, 2014; Vicente-Serrano *et al.*, 2015). Vicente-Serrano *et al.* (2015) found that climate drought indices have different sensitivities to the precipitation (P_r) and the potential evaporation (E_p) forcings. The Palmer Drought Severity Index (PDSI) has the lowest sensitivity to variation in climate inputs probably due to its standardization procedure for soil-water-budget-anomalies. The Standardized Precipitation Evapotranspiration Index (SPEI) shows equal sensitivity to P_r and E_p. Large uncertainties in drought trends primarily result from the choice of E_p parameterization in calculating drought indices (Sheffield *et al.*, 2012; Dai, 2013; Trenberth *et al.*, 2014; Yan *et al.*, 2014). For example, a PDSI model driven by solo air temperature (T_a)-based Thornthwaite E_p (1948) often overestimates the impact of drought due to temperature rising around most of the world (Sheffield *et al.*, 2012; Yan *et al.*, 2014).

Using drought-indices, several studies have been conducted on Chinese drought, especially under a background of warming. Nonetheless, different and even contrasting estimates of drought trends during 1980–2015 have been reported for China (Yu *et al.*, 2014; Chen and Sun, 2015; Li and Ma, 2015; Yan *et al.*, 2016; Chen *et al.*, 2017b; Shao *et al.*, 2018). Using a standard self-calibrating PDSI model driven with four atmospheric reanalysis data sets and station data, Shao *et al.* (2018) reported a significant drying trend across China from 1980 to 2015 with the drought area increasing by about 1.16% per decade. The 2005–2015 drought appeared to be the most prominent drought event. Based on land surface model-simulated soil moisture for the interval 1951–2008, Li and Ma (2015) reported China to have an increasing drought trend. Applying a SPEI model, Chen and Sun (2015) found that droughts became more frequent and severe across China from the late 1990s to 2012. Similarly by applying a SPEI model driven with Thornthwaite E_p (1948), Yu *et al.* (2014) pointed out that severe and extreme droughts became more serious for China from late 1990s to 2010. Chen *et al.* (2017b) has suggested a SPEI-model-based analysis indicates a wetting trend, but all PDSI indices show drying trends during 1961–2012 in China. However, Yan *et al.* (2016) reported an insignificant change of drought from 1982 to 2011 in China by using the self-calibrating PDSI$_{ARTS}$ model driven with climate data from 756 stations. These differences raise the question "What causes these contrasting estimates of the drying trend in China?" Considering the background of the temperature rising, we pose an additional question as to whether China had an extremely wet 5-year period occurred in the end of the past 35 years between 1982 and 2016.

The direct climatic cause of drought is below normal precipitation, which often results from anomalies of atmosphere circulation. Global sea surface temperatures have a teleconnection with summer drought in China (Zhang *et al.*, 2017). The El Niño-Southern Oscillation (ENSO) is regarded as the most important ocean–atmosphere system occurring over the tropical eastern Pacific Ocean. ENSO can change the global atmospheric circulation, which in turn, causes significant global temperature and precipitation anomalies.

El Niño events often increase precipitation over southern China (Zhang *et al.*, 1999; Dai and Wigley, 2000; Ma *et al.*, 2018). Strong anticyclonic-circulation anomalies persist in the northwestern Pacific and cause anomalously strong southerly water vapour transport to southern China through Walker circulation (Zhang *et al.*, 1999; Dai and Wigley, 2000; Zhai *et al.*, 2016). Extreme El Niño events, such as the 1997/1998 event, have incurred devastating floods over southern China due to abnormal rainfall (Chen *et al.*, 2018). The recent El Niño event in 2015/16 is thought to rival major previous El Niño events in 1982/83 and 1997/98 (L'Heureux et al., 2017; Chen et al., 2017a).

Unlike the earlier two El Niño events (Chen *et al.*, 2018), the 2015/16 El Niño event produced contrasting rainfall patterns in southern China. It also impacted seasonal changes of temperature and precipitation in China, for example, significant negative anomalies of summer precipitation in 2015 occurred in North China (Zhai *et al.*, 2016; Ma *et al.*, 2018), but its seasonal precipitation anomalies did not necessarily cause floods or extreme drought (Wang *et al.*, 2017; Ma *et al.*, 2018). The impact of the three El Niño events on the wetness and dryness changes in China on an interannual scale is not clear.

In this paper, the self-calibrating PDSI$_{ARTS}$ model (Yan *et al.*, 2014) was adopted to build a drought climatology at a spatial resolution of 8 km in China over the period of 35 years from 1982 to 2016. This paper includes following sections: (a) summary of PDSI$_{ARTS}$ model; (b) spatial and temporal analysis of PDSI$_{ARTS}$ drought across China over 1982–2016; (c) detection of the wettest period and analysis of related-climate factors over 2012–2016; (d) analysis of impacts of extreme El Niño events in1982/83, 1997/98, and 2015/16 on drought changes in China; (e) comparisons of PDSI$_{ARTS}$ with other drought products.

2 | METHODS

We applied the self-calibrating PDSI$_{ARTS}$ model (Yan *et al.*, 2014), which incorporates the self-calibrating PDSI model (Wells *et al.*, 2004) with the ARTS E_0 module and snow-melting module — to account for the effects of calibration coefficients, seasonal vegetation, and snow melting. The PDSI$_{ARTS}$ model has been applied to drought

study in China (Yan *et al.*, 2016) and over the global terrestrial surface (Yan *et al.*, 2014) for period of 1982–2011. A detailed description of the PDSI$_{ARTS}$ model can be found in Appendix A (Self-calibrating PDSI$_{ARTS}$ model) and in Yan *et al.* (2014). Its calibration interval used for this study covers the entire data period of 1982–2016. Table 1 shows the classification of dry and wet degree as defined by Palmer PDSI index adopted in this study.

3 | DATASETS AND PRE-PROCESSING

China has a spectrum of thermal climate zones distributed from south to north (i.e., tropical zone, subtropical zone, warm-temperate zone, and cold-temperate zone), as well as large spatial variability of annual precipitation decreasing from south to north and from east to west. Please note that the Taiwan region is not analysed in this study due to lack of available climate data.

TABLE 1 Classification of degree of wetness and dryness as defined by Palmer PDSI index

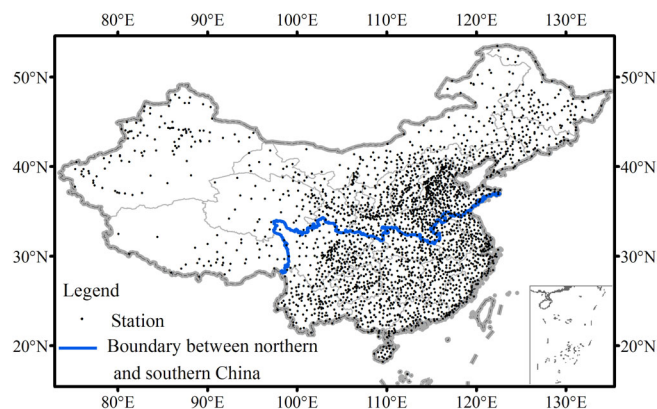| PDSI	Class	PDSI	Class
4.0 ≤ PDSI	Extremely wet	−1.0 to −0.5	Incipient drought
3.0 to 4.0	Very wet	−2.0 to −1.0	Mild drought
2.0 to 3.0	Moderately wet	−3.0 to −2.0	Moderate drought
1.0 to 2.0	Slightly wet	−4.0 to −3.0	Severe drought
0.5 to 1.0	Incipient wet spell	PDSI ≤ −4.0	Extreme drought
−0.5 to 0.5	Near normal		

FIGURE 1 Distribution of 2,000 high-density meteorological stations in China and the boundary showing northern China and southern China [Colour figure can be viewed at wileyonlinelibrary.com]

3.1 | Climate data

Monthly climate data (i.e., precipitation, air temperature, sunshine duration, wind speed, actual water vapour pressure, and relative humidity) at 2000 high-density weather stations across China for the period of 1982–2016 were collected from National Meteorological Information Center (NMIC) of Chinese Meteorological Administration (CMA). Currently, climate data from 824 stations is available at http://cdc.nmic.cn/home.do. Figure 1 shows the distribution of the 2000 high-density meteorological stations across China and the boundary between northern China and southern China. Most stations are concentrated over Eastern China, while Western China has a fewer stations. Thus, there may be higher uncertainties from spatial interpolation over regions with a low density of Western Chinese stations.

3.2 | Global inventory modelling and mapping studies (GIMMS) leaf area index data (version 4, 1981.7 ~ 2016.12)

The latest global leaf area index dataset (LAI3g), for the period from July 1981 to December 2016, was generated at 15-day temporal intervals and 8-km spatial resolutions from GIMMS Advanced Very High Resolution Radiometer (AVHRR) normalized difference vegetation index (NDVI) third generation (3 g) data set using an Artificial Neural Network (ANN) model (Zhu *et al.*, 2013). The remote-sensing L_{ai} time series data has been used in research of: Global drought monitoring and impacts of ENSO events (Yan *et al.*, 2014); Drought monitoring in China over 1982–2011 (Yan *et al.*, 2016); Investigating the weakening relationship between interannual temperature variability and northern vegetation activity (Piao *et al.*, 2010); Determining the interannual variability of global carbon cycle (Poulter *et al.*, 2014).

3.3 | Gridded soil database

The available water capacity (M_{awc}) for a soil depth of 0 to 150 cm, as required by the PDSI$_{ARTS}$ model, was adopted from the "Global Gridded Surfaces of Selected Soil Characteristics" data set developed by Global Soil Data Task Group (2000) of the International Geosphere-Biosphere Programme (IGBP)-Data and Information System (DIS). The data set contains seven parameters (available water capacity, soil-carbon density, total nitrogen density, field capacity, wilting point, thermal capacity, and bulk density) at a resolution of 5 arc-minutes, that is, 0.083°.
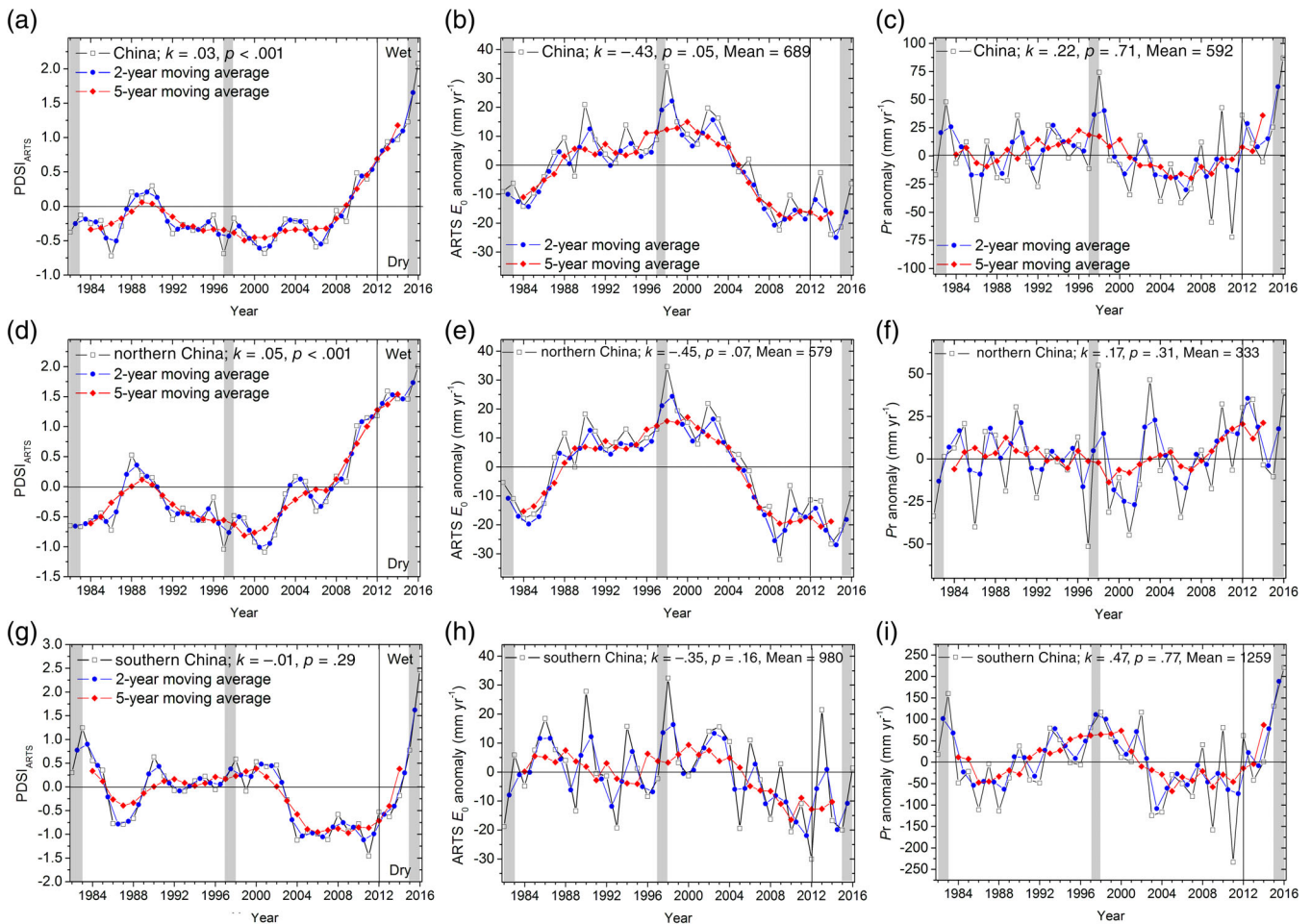
FIGURE 2 Time series of annual (a, d, g) average $PDSI_{ARTS}$, (b, e, h) ARTS E_0 anomaly, and (c, f, i) P_r anomaly in whole China (upper), northern China (middle), and southern China (bottom) during 1982–2016 relative to 1982–2011 mean. Shade shows three extreme El Niño events in 1982/83, 1997/98, and 2015/16 [Colour figure can be viewed at wileyonlinelibrary.com]

3.4 | Two available drought products

Two published drought products, that is, self-calibrating $PDSI_{CRU}$ (van der Schrier *et al.*, 2013) and SPEI at a time-scale of 24-month (Vicente-Serrano *et al.*, 2010) were downloaded for comparison with $PDSI_{ARTS}$. The $PDSI_{CRU}$ and SPEI products were derived from monthly P_r and Penman-Monteith E_p (E_{p_CRU}; Allen *et al.*, 1994) data from Climatic Research Unit (CRU) 0.5° gridded datasets (V4.03) at the University of East Anglia (UEA). The CRU dataset includes six climate variables, that is, mean temperature, diurnal temperature range, precipitation, wet-day frequency, vapour pressure, and cloud cover (Harris *et al.*, 2014). Since there is no monthly-mean-wind-speed data from 1901 onwards, the gridded 1961–1990 monthly normals for wind speed were adopted to calculate E_{p_CRU} (van der Schrier *et al.*, 2013; Harris *et al.*, 2014). CRU datasets included relatively less stations with no more than 400 stations in China.

3.5 | Data processing

All model forcing data including GIMMS L_{ai} data, meteorological data, and soil M_{awc} data were interpolated to the same 8 km spatial resolution. Meteorological data from 2000 high-density stations were interpolated using an Inverse Distance Weighted (IDW) interpolation method. As there is much less net radiation (R_n) observation across China, R_n was calculated from monthly mean sunshine duration, maximum (T_{max}) and minimum (T_{min}) air temperatures, and actual water vapour pressure according to the Food and Agriculture Organization (FAO) method (Allen, 1998).

L_{ai} and climate data were then applied to calculate ARTS E_0 and drive the self-calibrating $PDSI_{ARTS}$ model on a monthly scale. Similarly, Penman-Monteith potential evaporation (E_{P_PM}; Allen *et al.*, 1994) and the standard self-calibrating PDSI ($PDSI_{PM}$; Wells *et al.*, 2004) were calculated. The $PDSI_{ARTS}$ and $PDSI_{PM}$ were calibrated over
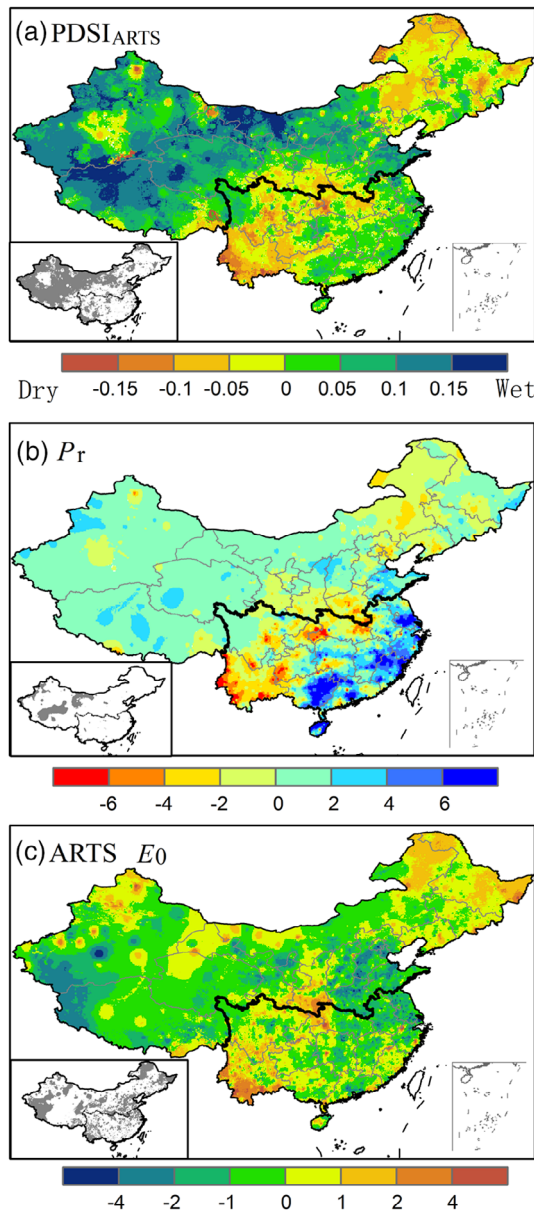
FIGURE 3 Linear trends of annual (a) average PDSI$_{ARTS}$, (b) P_r (mm yr^{-1}), and (c) ARTS E_0 (mm yr^{-1}) and their significance ($p < .05$ shown in grey colour in the hatch) of linear trend for period of 1982–2016, respectively [Colour figure can be viewed at wileyonlinelibrary.com]

the entire data period of 1982–2016. The PDSI$_{ARTS}$ drought climatology was then analysed against climate factors, PDSI$_{PM}$, and two available drought products (i.e., PDSI$_{CRU}$ and SPEI) for the same period of 1982 to 2016.

In this study, we used a linear regression for trend analyses in climate time series on an interannual scale:

$$y = k \times x + b \quad (1)$$

where y is a drought index or climate factor, x is time, k and b are the slope and intercept of the linear

regression, respectively (Mudelsee, 2019). The p value for the student t-test of the slope of k determined the significance of trend of drought indices and climate factors on an interannual scale, as suggested by Longobardi and Villani (2010). The slope of k represented the annual trends of drought indices or climate factors during the research interval.

4 | RESULTS

4.1 | A wetting trend in China from 1982 to 2016 and the wettest 5-year period of 2012–2016

China had a wetting trend ($p < .001$) with PDSI$_{ARTS}$ having a slope of $k = 0.03$ from 1982 to 2016 (Figure 2a). Similarly, northern China had a wetting trend ($p < .001$) with PDSI$_{ARTS}$ having a slope of $k = 0.05$ (Figure 2d). However, southern China had no significant change of drought during 1982–2016 (Figure 2g). Figure 2 shows P_r had a positive slope of k ($p > .05$) and ARTS E_0 had a negative slope of k ($p > .05$) for whole China, northern China, and southern China, respectively, that is, they had no significant trend. Their combined effects incorporating water supply and evaporation requirement, resulted in the wetting trend from 1982 to 2016 for whole China and northern China (Figure 2a,d). Similarly, the non-parametric Mann-Kendall test (Longobardi and Villani, 2010) was applied to significance test of PDSI$_{ARTS}$ trend, and also gave a wetting trend in China ($p < .05$) and northern China ($p < .01$) over 1982–2016.

Some studies (Sun and Yang, 2012; Lu et al., 2014; Xu et al., 2014) indicate that a once-in-a-fifty-year severe drought swept southern China in 2011. This was confirmed by our study. The 2011 drought was the driest event occurred over southern China during 1982–2016 with PDSI$_{ARTS}$ = −1.4 (Figure 2g) due to the lowest P_r (Figure 2i).

Figure 3a shows that the wetting trend was significant ($p < .05$) in northwestern China with PDSI$_{ARTS}$ having a slope of k higher than 0.05 from 1982 to 2016, while northeast China and southern China had no significant change of drought. Figure 3b,c shows that P_r had a positive slope of k and ARTS E_0 had a negative slope of k for most China. Northwestern China features arid climate, but became wetter under the background of warming, which differs from the concept that "dry regions get drier, and wet regions become wetter" as a result of global water cycle intensification in response to warming (Held and Soden, 2006; Feng and Zhang, 2016). In deed Donat et al. (2016) suggested that dry regions across the world, for example, northwestern China, received more precipitation during the period of 1981 to 2010 due to global
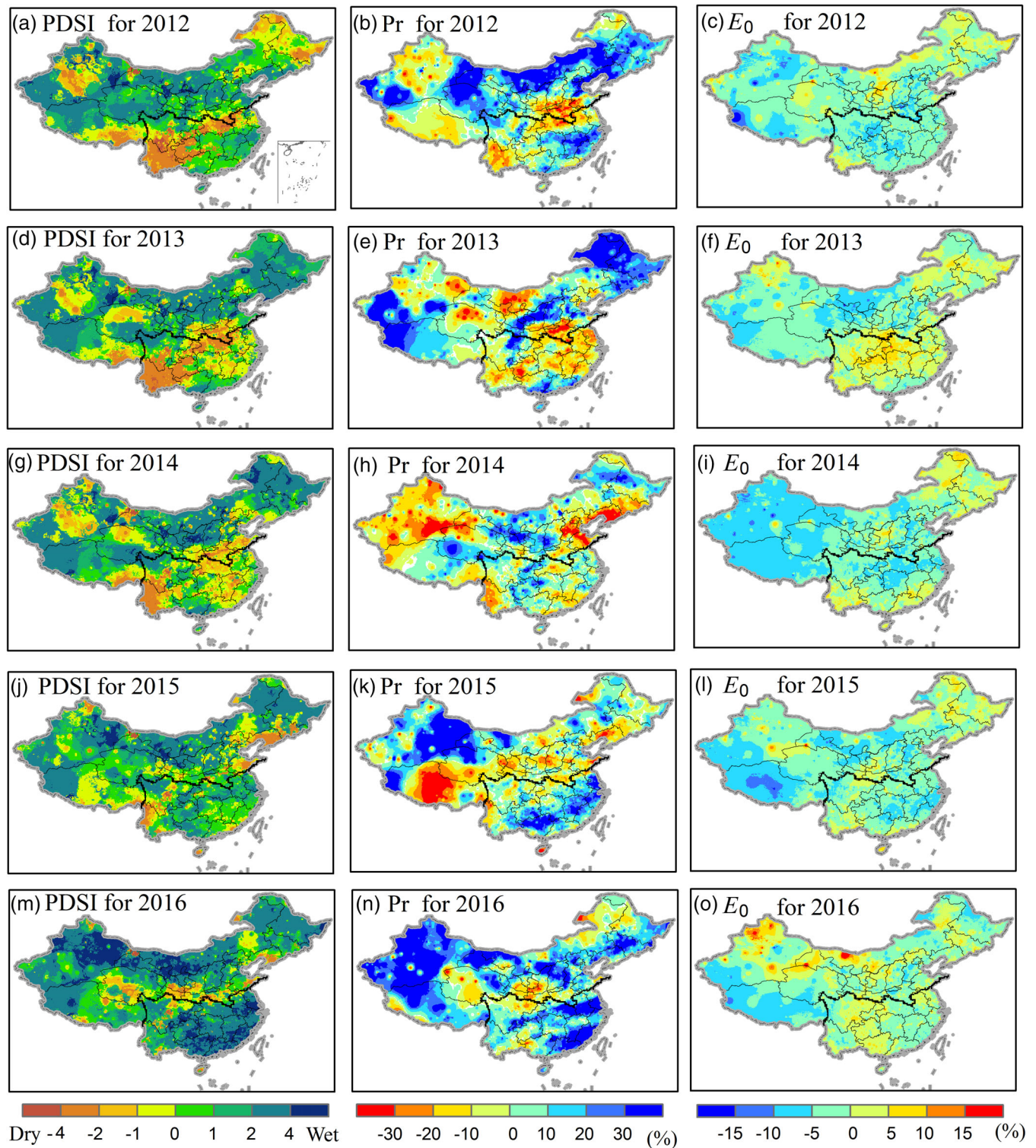
FIGURE 4 Annual (left) average $PDSI_{ARTS}$, and anomaly percentage of (middle) P_r (mm yr^{-1}) and (right) ARTS E_0 (mm yr^{-1}) from (top) 2012 to (bottom) 2016, respectively. The black line shows the boundary between northern China and southern China [Colour figure can be viewed at wileyonlinelibrary.com]

warming-related precipitation intensification, which was confirmed by this study (Figure 3b).

Five year-moving average $PDSI_{ARTS}$ shows that the whole of China (Figure 2a) had the wettest 5-year period in 2012–2016 with an average $PDSI_{ARTS}$ of 1.2. For China, this was mainly attributed to weak evaporation demand (Figure 2b) and sufficient water supply (Figure 2c) during 2012–2016 with annual ARTS E_0 having a negative

anomaly (ΔE_0) of -22.5 mm yr^{-1} and annual P_r having a positive anomaly (ΔP_r) of 36.1 mm yr^{-1} relative to 1982–2011 mean, respectively. The annual P_r in 2016 was 684.2 mm recorded as the highest P_r in China during the past 35-year period of 1982–2016.

For this, the wettest 5-year interval (2012–2016), annual mean T_a increased by 0.5 °C compared with annual climate mean T_a of 9.3°C averaged over 30 years of 1982–2011. However, annual mean S_p, W_s, and R_h of 2012–2016 decreased by -1.0%, -0.07 m s^{-1}, and -2.1% compared with annual climate means over 1982–2011, respectively. These offset the impact of the temperature increase and produced the weak potential evaporation of ARTS E_0 during 2012–2016 in China.

Similarly, northern China (Figure 2d) had the wettest 5-year period of 2012–2016 due to weak evaporation demand (Figure 2e) with $\Delta E_0 = -18.8$ mm yr^{-1} and plentiful precipitation (Figure 2f) with $\Delta P_r = 21.2$ mm yr^{-1} averaged over 2012–2016. For southern China (Figure 2g), a rather wet 5-year period of 2012–2016 was observed with an average PDSI$_{ARTS}$ of 0.4, an average ΔP_r of 86.8 mm yr^{-1} (Figure 2i), and an average ΔE_0 of -10.3 mm yr^{-1} (Figure 2h), respectively. Southern China also recorded the highest P_r of 1,492.6 mm in 2016 during the past 35-year period of 1982–2016.

Figure 4 explicitly shows the annual average PDSI$_{ARTS}$, and the anomaly percentage of annual P_r and ARTS E_0 from 2012 to 2016, respectively. Area percentages (Table 2) show that more than 49% of land area of China experienced wetter conditions with PDSI$_{ARTS} > 1$

TABLE 2 Area percentage (%) of land with PDSI$_{ARTS} > 1$, $\Delta P_r > 0$, and ΔARTS $E_0 < 0$ for 2012–2016 relative to the 1982–2011 mean in China, respectively

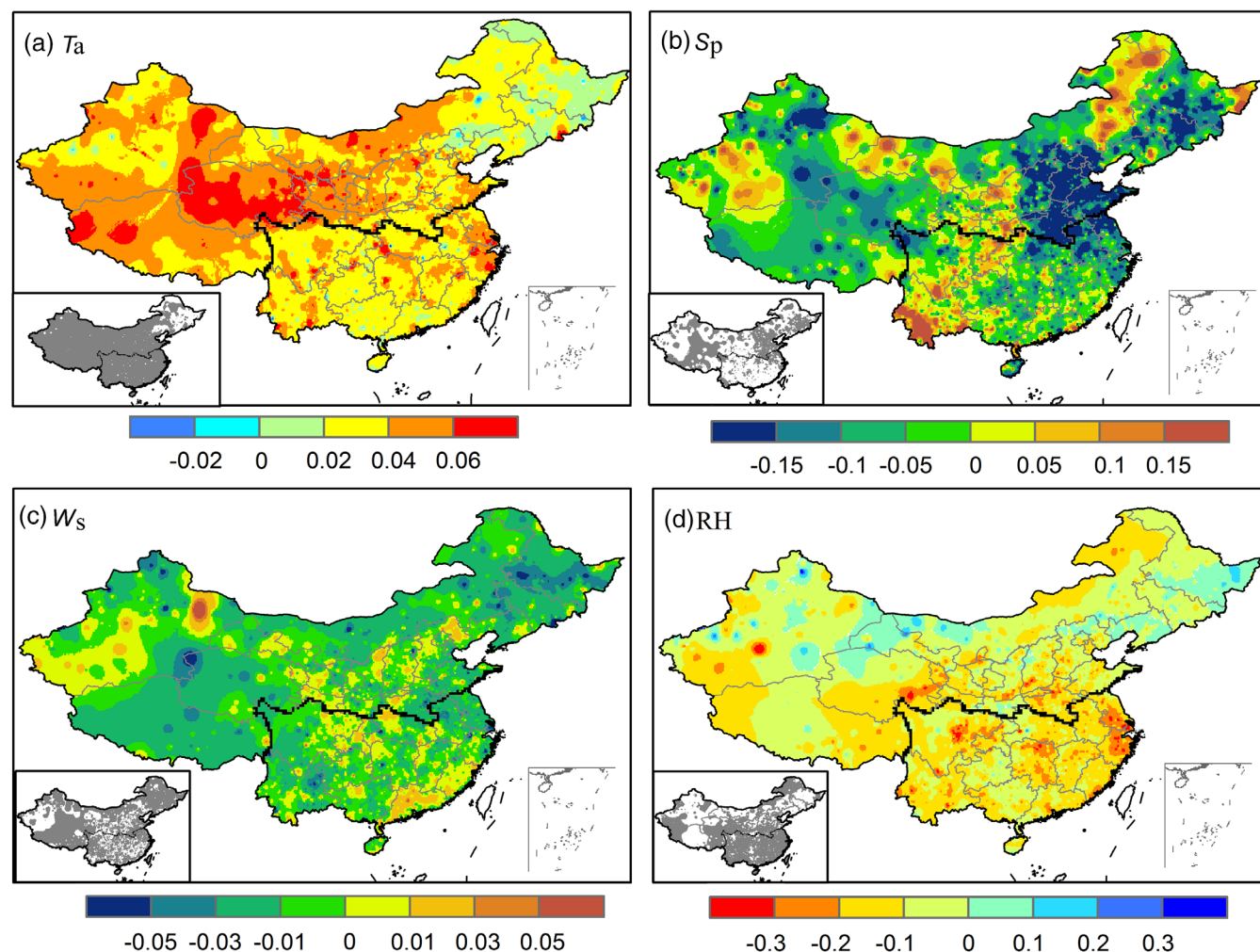| Year	2012	2013	2014	2015	2016
PDSI$_{ARTS} > 1$	49%	54%	53%	57%	74%
$\Delta P_r > 0$	61%	54%	44%	54%	75%
ΔARTS $E_0 < 0$	71%	57%	75%	73%	54%

FIGURE 5 Linear trends of annual average (a) T_a, (b) surface sunshine percent S_p, (c) W_s, and (d) R_h and their significance ($p < .05$ shown in grey colour in the hatch) in China during 1982–2016 [Colour figure can be viewed at wileyonlinelibrary.com]

for all 5 years. More than 50% of land area of China received plentiful P_r with $\Delta P_r > 0$ for 4 years, with an exception of 2014 (44%). Over 54% of land area of China had weak potential evaporation with $\Delta E_0 < 0$ for all 5 years. This was particularly so for year 2016, which was the wettest year during the past 35 years of 1982–2016. In 2016, 74% of land area of China was wetter than normal ($PDSI_{ARTS} > 1$)—corresponding to 75% of land area of China receiving ample P_r with $\Delta P_r > 0$

and 54% of land area of China having an reduced evaporation demand with $\Delta E_0 < 0$.

4.2 | Interannual changes of evaporation factors during 1982–2016

Between 1982–2016, the annual average T_a increased by 0.2°C~0.6°C per decade in most China, especially in western
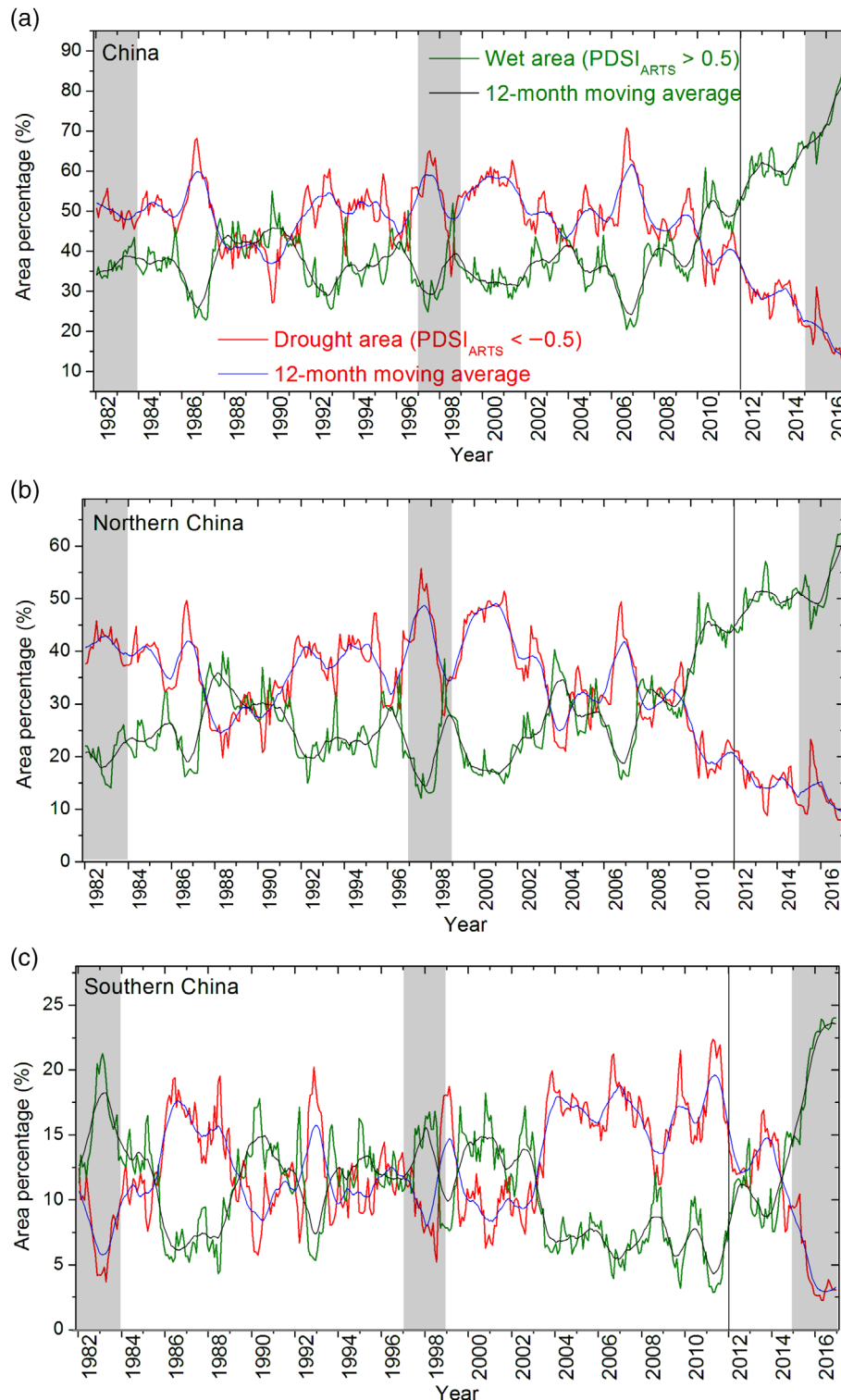

FIGURE 6 Time series of monthly area percentage (%) of drought land with $PDSI_{ARTS} < -0.5$ and wet land with $PDSI_{ARTS} > 0.5$ in (a) China, (b) northern China, and (c) southern China during 1982–2016. Shade shows three extreme El Niño events in 1982/83, 1997/98, and 2015/16 [Colour figure can be viewed at wileyonlinelibrary.com]

China (Figure 5a). T_a increased by 0.38°C per decade ($p < .001$) for whole China. Figure 5b shows that most regions had a decreasing trend of S_p by −1.5% to −0.5% per decade, and S_p decreased by −0.39% per decade ($p < .01$) for whole China during 1982–2016. As T_a and sunlight are important energy factors affecting potential

evaporation according to Penman-Monteith evaporation theory (Monteith, 1965), the decreasing trend of S_p offset the impact of the increasing trend of T_a in calculating ARTS E_0 for the period of 1982–2016. The observed decreases in the monthly percentage of sunshine duration, and global radiation and direct radiation partially resulted from increased

FIGURE 7 Time series of monthly area percentage (%) of wet land defined by PDSI$_{ARTS}$ in China during 1982–2016 [Colour figure can be viewed at wileyonlinelibrary.com]

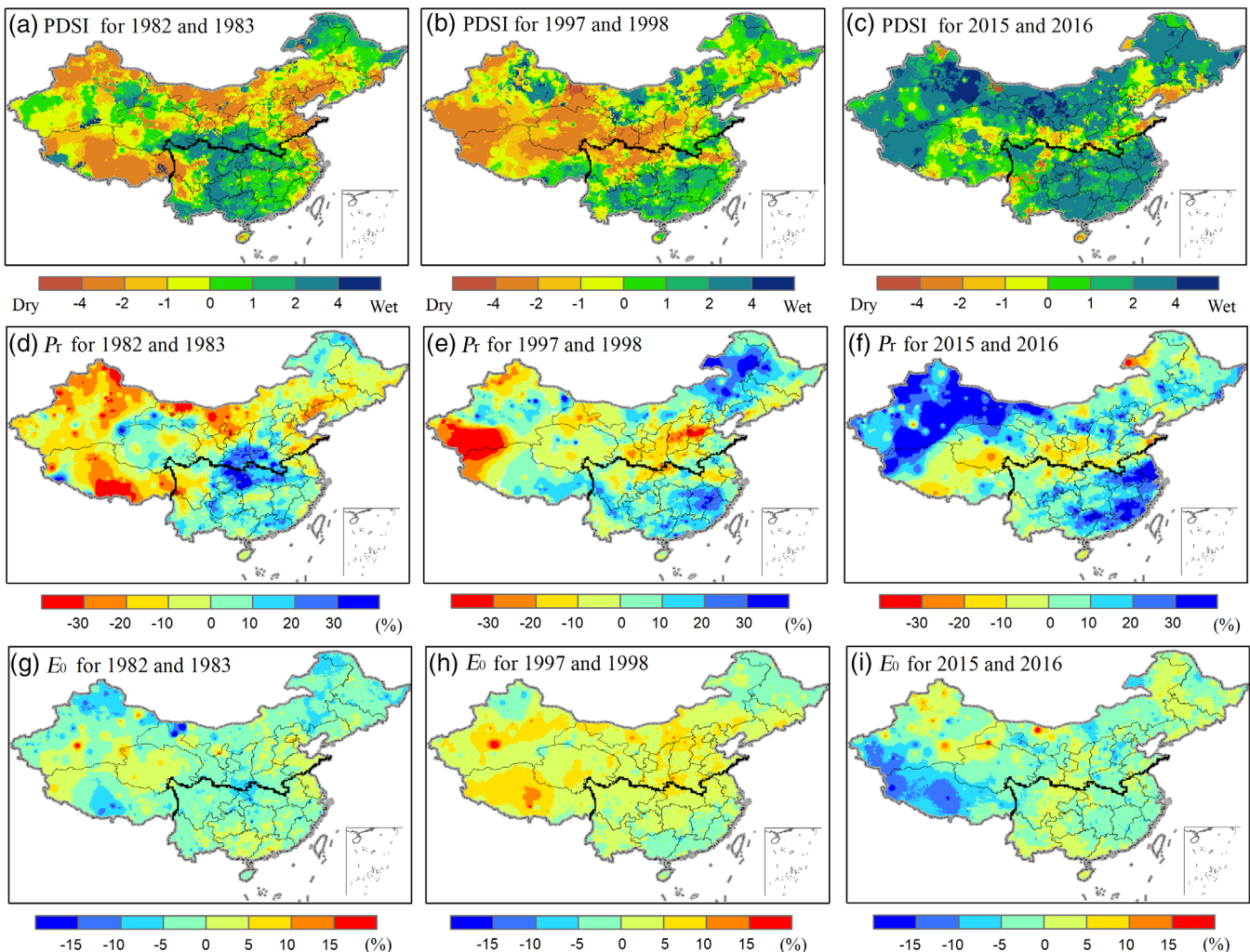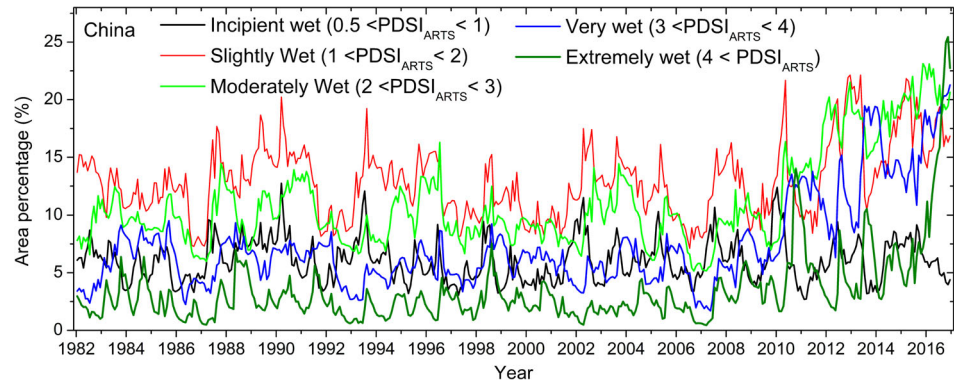**FIGURE 8** Spatial pattern of annual (a–c) average PDSI$_{ARTS}$, anomaly percentage of (d–f) P_r and (g–i) ARTS E_0 for three extreme El Niño events in (left) 1982/83, (middle) 1997/98, and (right) 2015/16 over China [Colour figure can be viewed at wileyonlinelibrary.com]

aerosol pollution in China (Che *et al.*, 2005; Yang *et al.*, 2016).

Similarly, wind speed W_s was an aerodynamic factor (Monteith, 1965) that decreased by 0.1 m s^{-1} per decade ($p < .001$) during the research period. Most regions in China had a decreasing trend of W_s by -0.5 m s^{-1} to -0.1 m s^{-1} per decade (Figure 5c), which agreed with published studies (Wu *et al.*, 2017). The decreasing trend of surface wind speed is attributed to changes in the driving forces caused by atmosphere circulation, and changes in the drag forces such as surface friction due to land use and land cover change (Wu *et al.*, 2017).

As R_h is a key variable in calculating plant transpiration and soil evaporation of ARTS E_0 (Yan *et al.*, 2016), Figure 5d shows that most regions had a decreasing trend of R_h by -3% to -0.5% per decade, and R_h decreased by 0.9% per decade ($p < .001$) across all of China.

4.3 | Monthly changes of drought and wet area from 1982–2016

Based on the classification of wetness and dryness as defined by Palmer PDSI index (Table 1), we calculated monthly wet area with PDSI$_{ARTS}$ > 0.5 and drought area with PDSI$_{ARTS}$ < -0.5 during 1982–2016. Figure 6a,b indicates that for both whole China and northern China, the drought area was often higher than the wet area before 2010, but this was reversed after 2010 with the wet area becoming higher than the drought area. Figure 6a also shows that for China the wet area gradually increased from 21% in 2006 to 86% in 2016, while the drought area decreased from 70% in 2006 to 12% in 2016 in China. Similarly, for northern China (Figure 6b), the wet area gradually increased from 15% in 2006 to 60% in 2016,

while the drought area decreased from 50% in 2006 to 10% in 2016.

For southern China (Figure 6c), the drought area was often higher than the wet area during 2003–2014. After 2014, the wet area became higher than the drought area. Wet area increased from 3% in 2011 to 23% in 2016, while drought area decreased from 22% in 2011 to 2% in 2016. In addition, area percentages at five levels of wetness, from Incipient wet to Extreme wet (Table 1), were produced (Figure 7). It shows that the Incipient wet area had no trend ($p = .77$) during 1982–2016. Other four types of wet areas, from the Slightly wet to the Extremely wet, all had an increasing trend ($p < .0001$).

4.4 | Impact of extreme El Niño events

Three extreme El Niño events caused positive rainfall anomalies of 89 mm yr^{-1}, 98 mm yr^{-1}, and 175 mm yr^{-1} in 1982/83, 1997/98, and 2015/16 over southern China,

TABLE 3 Linear trend k and significance p of annual average PDSI$_{ARTS}$, P_r, and ARTS E_0 for periods of 1982–2016, 1982–2014, and 1982–2011 in China

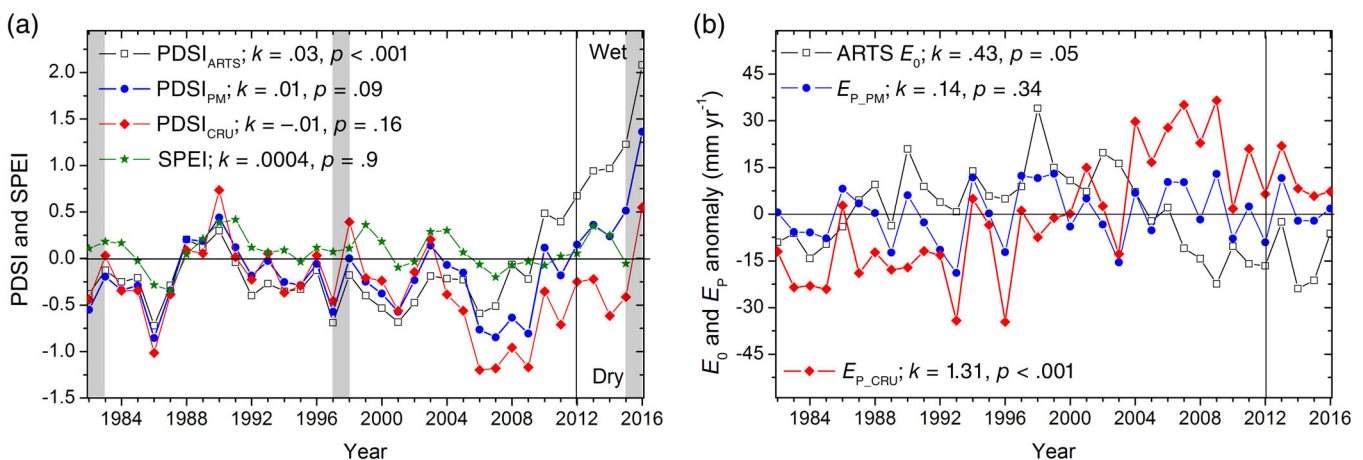| Time period	PDSI$_{ARTS}$	P_r	ARTS E_0
1982–2016	$k = 0.032$ ($p < .001$)	$k = 0.22$ ($p = .71$)	$k = -0.43$ ($p = .05$)
1982–2014	$k = 0.018$ ($p < .05$)	$k = -0.40$ ($p = .50$)	$k = -0.35$ ($p = .15$)
1982–2011	$k = 0.003$ ($p = .65$)	$k = -0.89$ ($p = .20$)	$k = -0.13$ ($p = .63$)

FIGURE 9 Time series of annual (a) average PDSI$_{ARTS}$, PDSI$_{PM}$, PDSI$_{CRU}$, and SPEI, and (b) anomaly of ARTS E_0, E_{P_PM}, and E_{P_CRU} in China during 1982–2016 relative to 1982–2011 mean. Shade shows three extreme El Niño events in 1982/83, 1997/98, and 2015/16 [Colour figure can be viewed at wileyonlinelibrary.com]

respectively. Figure 8d–f shows that most regions in southern China observed positive anomalies of P_r during the three El Niño events. As a result, southern China often had a wet climate with average PDSI higher than 0.5 (Figure 8a–c) and with wet area higher than drought area (Figure 6c) during the three extreme El Niño events.

However, large differences existed in impacts of the three El Niño events. The 2015/16 interval featured the highest annual P_r in southern China among three El Niño events, and the highest area with positive anomalies of $P_r > 10\%$ in southern China and northern China (Figure 8f). In addition, evaporative factor E_0 indicates that 2015/16 and 1982/83 intervals had more areas with
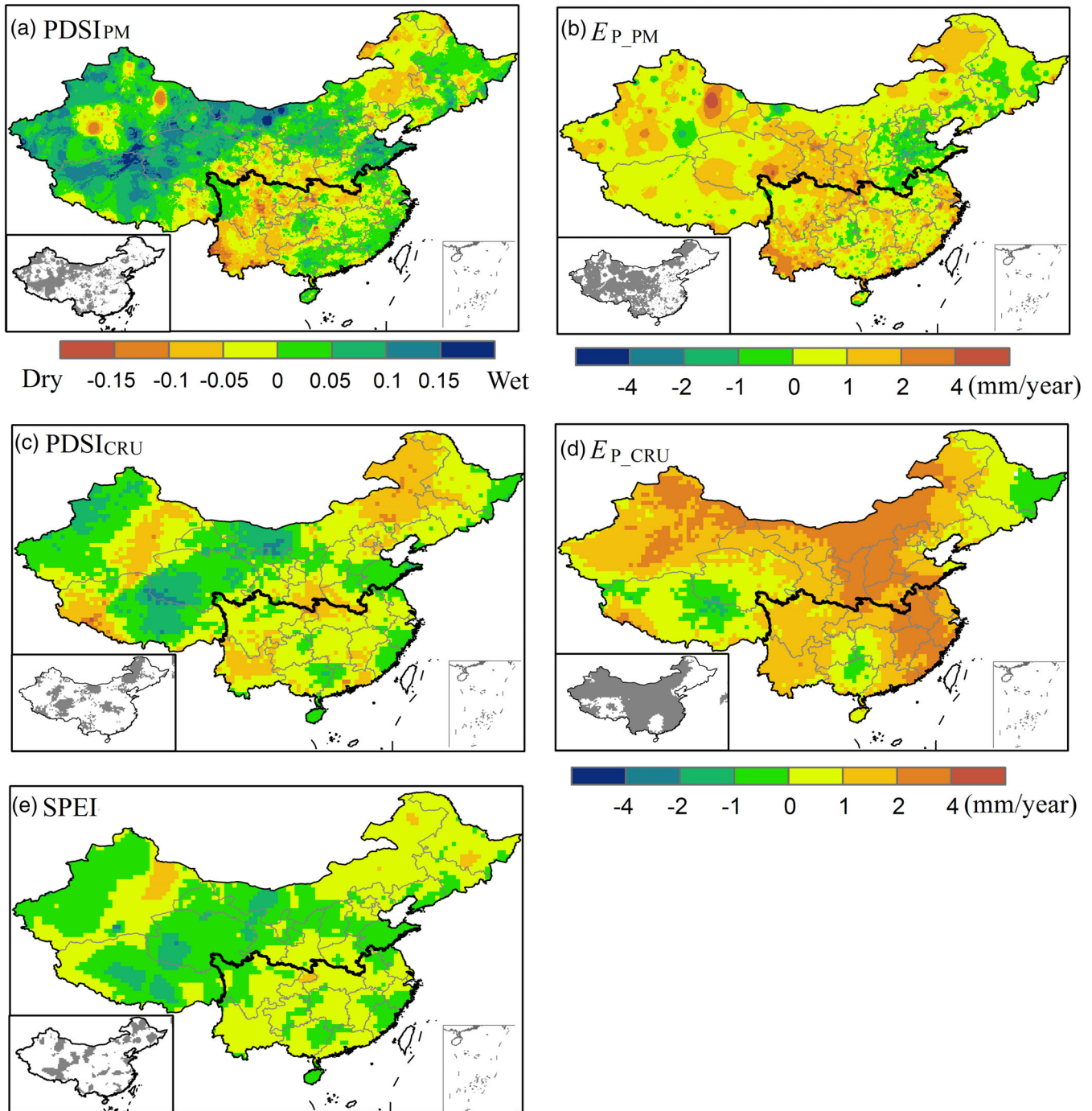

FIGURE 10 Linear trends of annual (a) average PDSI$_{PM}$, (b) E_{P_PM} (mm yr^{-1}), (c) PDSI$_{CRU}$, (d) E_{P_CRU} (mm yr^{-1}), (e) SPEI, and their significance ($p < .05$ shown in grey colour in the hatch) of linear trend for period of 1982–2016, respectively [Colour figure can be viewed at wileyonlinelibrary.com]

negative anomalies of E_0 than 1997/98 interval in southern China (Figure 8g–i). As a coupled effect of P_r and E_0, the 2015/16 El Niño event produced the wettest climate in southern China and contributed to the wettest 2-year of 2015/16 in China during the past 35 years of 1982–2016.

In contrast to southern China, northern China observed rainfall anomalies of -16.1 mm yr^{-1}, 1.8 mm yr^{-1}, and 14.7 mm yr^{-1} in 1982/83, 1997/98, and 2015/16, respectively, which shows no simple relationship between extreme El Niño events and rainfall anomalies in northern China. Figure 8f also indicates that most northern China had positive rainfall anomalies in 2015/16 while negative rainfall anomalies spread over most northern China in 1982/83 (Figure 8d). Further, northern China had more areas experiencing positive anomalies of E_0 in the 1997/98 interval compared with 2015/16 and 1982/83 intervals (Figure 8g–i). These joint impacts of P_r and E_0 resulted in the wettest climate in northern China in 2015/16 among the three El Niño events. For the whole of China, 81% of land area in China had a positive value of PDSI in the wettest 2-year of 2015–2016 due to abundant P_r and weak E_0 (Figure 8c). Excluding the impact of the 2015/16 El Niño event, China still had a wetting trend ($p < .05$) for the shortened period of 1982–2014 (Table 3). The 2015/16 El Niño event intensified the wetting trend ($p < .001$) from 1982 to 2016 arising from the increasing P_r and the decreasing evaporation of ARTS E_0 (Table 3).

4.5 | Comparisons with two drought products

PDSI$_{CRU}$ and SPEI had a nonsignificant trend ($p > .1$) in China (Figure 9). E_{P_CRU}, as a key driving data adopted by these two indices, had an increasing trend ($k = 1.31$; $p < .001$) for 1982–2016 (Figure 9b), which offset the impact of increasing P_r ($k = 0.22$; $p = .71$) and produced the nonsignificant trend in PDSI$_{CRU}$ and SPEI, different from the wetting trend of PDSI$_{ARTS}$.

Using the 2000-station dataset in China and the standard self-calibrating PDSI model (Wells *et al.*, 2004),

E_{P_PM} and its corresponding PDSI$_{PM}$ were calculated for 1982–2016. Figure 9 shows that E_{P_PM} had a nonsignificant trend ($k = 0.14$, $p = .34$), and PDSI$_{PM}$ also had no significant trend ($k = 0.01$, $p = .09$), consistent with PDSI$_{CRU}$ in China.

Figure 9a also indicates that PDSI$_{ARTS}$ detected the driest two-year era in 2000 and 2001 during the period of 1982–2016, while PDSI$_{CRU}$ and PDSI$_{PM}$ detected the driest two-year era occurred in 2006 and 2007, and SPEI had the driest two-year era in 1986 and 1987.

Figure 9a indicates that PDSI$_{ARTS}$, PDSI$_{CRU}$, and PDSI$_{PM}$ all showed a "jump" (i.e., a fast wetting trend) from 2006 to 2016. This was attributable to a decreasing trend of ARTS E_0, E_{P_PM}, and E_{P_CRU} from 2006 to 2016 (Figure 9b) coupled with the increasing P_r for the same period. However, SPEI did not show the "jump" from 2006 to 2016.

Although PDSI$_{PM}$ and PDSI$_{CRU}$ were calculated with the same E_P equation (Allen *et al.*, 1994) and self-calibrating PDSI model (Wells *et al.*, 2004), Figure 10 shows that PDSI$_{PM}$ identified more areas with a wetting trend when compared with PDSI$_{CRU}$ and SPEI in China. E_{P_PM} (Figure 10b) and E_{P_CRU} (Figure 10d) were different, and E_{P_CRU} trends were overestimated relative to E_{P_PM} trends for 1982–2016. This difference primarily resulted from the use of different driving forcing in calculating E_P, for example, different wind speed data, radiation data, and observation stations.

5 | DISCUSSION AND CONCLUSIONS

As northern China occupies 2.6 times the area of southern China, the dry/wet changes in whole China when averaged are dominated by northern China. We found that significant wetting occurred in entire China and the northern China region from 1982 to 2016 mainly due to coupled effects of decreasing E_0 and increasing precipitation, which suggests that temperature rising did not result in an increasing trend of drought in China in the past. As a result, the 5-year period of 2012–2016 was the

TABLE 4 Correlation coefficient R and significance level p of annual average PDSI$_{ARTS}$ against annual P_r and ARTS E_0 for 1982–2016 in northern China and southern China, respectively. Five year moving average PDSI$_{ARTS}$ (i.e., PDSI$_{ARTS}$ of 5 yr) was also analysed against 5 year moving average P_r and E_0

	Northern China		Southern China	
	P_r	E_0	P_r	E_0
PDSI$_{ARTS}$	$R = 0.49$ ($p < .005$)	$R = -0.48$ ($p < .005$)	$R = 0.74$ ($p < .0001$)	$R = 0.14$ ($p = .43$)
	P_r of 5 yr	E_0 of 5 yr	P_r of 5 yr	E_0 of 5 yr
PDSI$_{ARTS}$ of 5 yr	$R = 0.84$ ($p < .0001$)	$R = -0.74$ ($p < .0001$)	$R = 0.82$ ($p < .0001$)	$R = 0.54$ ($p < .005$)

wettest era in the past 35 years (1982–2016) in China. China maintained a wetting trend for 1982–2014, while the 2015/16 El Niño event only intensified this wetting trend.

Dominant climate factors in determining drought trends varied with climatological zones. In northern China's dry climate, annual average $\text{PDSI}_{\text{ARTS}}$ had a positive relationship ($R = 0.49$, $p < .005$) with P_r and a negative relationship ($R = -0.48$, $p < .005$) with ARTS E_0 (Table 4). E_0 played a role approximating to P_r in determining drought changes in northern China because E_0 and P_r anomalies had a similar changing amplitude from -30 mm yr^{-1} to 30 mm yr^{-1} during 1982–2016 (Figure 2e,f).

However, with southern China having a rather humid climate, annual average $\text{PDSI}_{\text{ARTS}}$ had a positive relationship ($R = 0.74$, $p < .0001$) with P_r and an insignificant relationship ($p = .43$) with ARTS E_0. This was because drought in southern China was mainly determined by P_r, which had an amplitude ranging from -150 mm yr^{-1} to 150 mm yr^{-1}. Meanwhile, the ARTS E_0 anomaly had an amplitude ranging from -25 mm yr^{-1} to 25 mm yr^{-1} in southern China during 1982–2016 (Figure 2h,i). The five year-moving average shows similar results (Table 4).

Debates concerning drought trends in China may arise from the use of different approaches and different input data to construct the drought index (Yu *et al.*, 2014; Chen and Sun, 2015; Li and Ma, 2015; Yan *et al.*, 2016; Chen *et al.*, 2017b; Shao *et al.*, 2018). For example, two published drought products, that is, PDSI_{CRU} and SPEI, indicate an insignificant trend in China during 1982–2016 using the CRU 0.5° gridded datasets, which differs from the wetting trend shown by $\text{PDSI}_{\text{ARTS}}$ using 2000 station-interpolated data. Self-calibrating PDSI and SPEI models are sensitive to the definition of potential evaporation as a model forcing (van der Schrier *et al.*, 2011). Here, PDSI_{CRU} and SPEI products were derived from Penman-Monteith E_p ($E_{\text{p\_CRU}}$; Allen *et al.*, 1994), while $\text{PDSI}_{\text{ARTS}}$ products were calculated from ARTS E_0 (Yan *et al.*, 2014).

Different calibration periods can produce different PDSI values (Wells *et al.*, 2004). van der Schrier *et al.* (2013) suggests adopting the full record of data as the calibration period so that impacts of the most severe droughts and pluvials are contained in the PDSI products. Our study focuses on the intercomparison of drought indices from 1982 to 2016, and the $\text{PDSI}_{\text{ARTS}}$ products use a calibration period from 1982 to 2016. However, the published PDSI_{CRU} products use a long calibration period from 1901 to 2018. The differences in calibration periods may have some impacts on the intercomparison of drought indices from 1982 to 2016 considered here.

The $\text{PDSI}_{\text{ARTS}}$ model had been applied to drought study for 1982–2011 in China driven with climate data at a resolution of 0.25° × 0.25° interpolated from 756 station data across China (Yan *et al.*, 2016), which shows nonsignificant change of drought over 1982–2011 in China. This study adopted 8 km-resolution climate data interpolated from 2000 high-density stations over 1982–2016, which should provide more reliable results—because more station data located in western China supplying the opportunity check the earlier results derived from 756 station data in previous study of Yan *et al.* (2016). This study initially found the wettest five year period of 2012–2016 and a wetting trend from 1982 to 2016 due to coupled effects of increased precipitation and decreased potential evaporation. This study also analysed impacts of El Niño events on drought changes in China.

Extreme El Niño events in 1982/83, 1997/98, and 2015/16 significantly increased P_r and further produced a wetter climate in southern China. However, the 2015/16 El Niño event differed from 1982/83 and 1997/98 El Niño events in that the 2015/16 event featured the highest annual P_r in southern China among three El Niño events, and most northern China had positive rainfall anomalies in 2015/16 interval. The 2-year period of 2015/2016 was the wettest two-year era in both northern China and southern China during the past 35 years.

The dynamics of climate system is very complex. The mechanism producing the wettest 2-year of 2015/16 during 1982–2016 in China is not clear. ENSO affects global climate, but this relationship is modulated by the Pacific Decadal Oscillation (PDO) (Ouyang *et al.*, 2014; Wang *et al.*, 2014). Analysis of the combined impacts of ENSO and PDO for the period 1900–2010 shows that El Niño events during PDO warm phase often enhance P_r (i.e., wet anomalies) in southern China and decrease P_r (i.e., dry anomalies) in northern China (Ouyang *et al.*, 2014; Wang *et al.*, 2014), which was supported by 1982/83 and 1997/98 extreme El Niño events in this study. However, we found that the 2015/16 extreme El Niño event even in PDO warm phase featured the highest P in both northern and southern China during the past 35 years. This differs from the earlier two extreme El Niño events and needs further research from a new perspective besides ENSO and PDO.

Considering the coupled effects of precipitation and potential evaporation, the PDSI drought index can indicate seasonal drought and wet conditions (Table 1; Palmer, 1965), and several applications investigating drying and wetting trends on interannual scales have been developed (Sheffield *et al.*, 2012; Dai, 2013; Trenberth *et al.*, 2014; Yan *et al.*, 2014). The PDSI_{PM} index shows a spatial mixture of drying, wetting, and nonsignificant trends across the global land surface, which combine to give a non-significant trend of global drought over 1980–2008 (Sheffield *et al.*, 2012). Yan *et al.* (2014) found

that global land became wetter for 1982–2011 mainly due to increased precipitation and ENSO effect by using PDSI$_{PM}$ and PDSI$_{ARTS}$ indices. For China, this study detected an overall wetting trend ($p < .001$ for t test and $p < .05$ for Mann-Kendall test) from 1982 to 2016 based on annual average PDSI$_{ARTS}$ index.

Drought trend, in essence, was determined by coupled effects of precipitation trend and potential evaporation trend, and a single wet event, such as an extreme El Niño event, did not result in a wetting trend for whole China or southern China. For instance, the 2015/16 El Niño event induced the highest P_r in southern China over 1982–2016, but southern China still had an insignificant change of drought during 1982–2016. Excluding the impact of 2015/16 El Niño event, China still maintained a wetting trend ($p < .05$) during the shortened 1982–2014 interval.

Global warming is expected to increase the frequency and intensity of droughts in the 21st century with most global land becoming drying (Cook *et al.*, 2014; Carrão *et al.*, 2018). However, based on SPEI and PDSI driven with the coupled Model Intercomparison Project Phase 5 (CMIP5) data (Cook *et al.*, 2014), the northern hemisphere high latitudes will experience robust wetting. In addition, CMIP5 predicted that global land including China may have more precipitation in the 21st century (Chen and Frauenfeld, 2014; Touma *et al.*, 2015) and precipitation-based Standardized Precipitation Index (SPI) reveals no significant changes of severe drought area. However, SDDI index (defined as precipitation minus E_p) predicts a stronger drought than SPI due to great influence of temperature rising in the E_p and SDDI index (Touma *et al.*, 2015), which shows large uncertainties in current projections of drying trend in the future because the projections heavily depends on the adopted drought indices and their parameterization of E_p. Under the background of increasing precipitation and temperature in the future, the likelihood of extreme wet period still exists.

More effects should be applied to analysis of historic drought and possible climate forcings to gain mechanistic insight into drought/wet changes. Only in light of reliable drought climatology, we can foresee drought variations and its impacts in the warming future with reduced uncertainties.

ORCID

Hao Yan https://orcid.org/0000-0002-5287-3298

REFERENCES

Allen, R.G. (1998) *Crop Evapotranspiration: Guidelines for Computing Crop Water Requirements*. Rome, Italy: Food and Agriculture Organization of the United Nations.

Allen, R.G., Smith, M., Pereira, L.S. and Perrier, A. (1994) An update for the calculation of reference evapotranspiration. *ICID Bulletin*, 43, 35–92.

Carrão, H., Naumann, G. and Barbosa, P. (2018) Global projections of drought hazard in a warming climate: a prime for disaster risk management. *Climate Dynamics*, 50, 2137–2155. https://doi.org/10.1007/s00382-017-3740-8.

Che, H.Z., Shi, G.Y., Zhang, X.Y., Arimoto, R., Zhao, J.Q., Xu, L., Wang, B. and Chen, Z.H. (2005) Analysis of 40 years of solar radiation data from China, 1961–2000. *Geophysical Research Letters*, 32, L06803. https://doi.org/10.1029/2004GL022322.

Chen, H. and Sun, J. (2015) Changes in drought characteristics over China using the standardized precipitation evapotranspiration index. *Journal of Climate*, 28, 5430–5447. https://doi.org/10.1175/JCLI-D-14-00707.1.

Chen, J., Wang, X., Zhou, W., Wang, C., Xie, Q., Li, G. and Chen, S. (2018) Unusual rainfall in southern China in decaying august during extreme El Niño 2015/16: role of the Western Indian Ocean and north tropical Atlantic SST. *Journal of Climate*, 31, 7019–7034. https://doi.org/10.1175/JCLI-D-17-0827.1.

Chen, J.M., Blanken, P.D., Black, T.A., Guilbeault, M. and Chen, S. (1997) Radiation regime and canopy architecture in a boreal aspen forest. *Agricultural and Forest Meteorology*, 86, 107–125. https://doi.org/10.1016/S0168-1923(96)02402-1.

Chen, L. and Frauenfeld, O.W. (2014) A comprehensive evaluation of precipitation simulations over China based on CMIP5 multimodel ensemble projections. *Journal of Geophysical Research: Atmospheres*, 119, 5767–5786. https://doi.org/10.1002/2013JD021190.

Chen, L., Li, T., Wang, B. and Wang, L. (2017a) Formation mechanism for 2015/16 super El Niño. *Scientific Reports*, 7, 2975. https://doi.org/10.1038/s41598-017-02926-3.

Chen, T., Zhang, H., Chen, X., Hagan, D.F., Wang, G., Gao, Z. and Shi, T. (2017b) Robust drying and wetting trends found in regions over China based on Köppen climate classifications. *Journal of Geophysical Research: Atmospheres*, 122, 4228–4237. https://doi.org/10.1002/2016JD026168.

Cook, B.I., Smerdon, J.E., Seager, R. and Coats, S. (2014) Global warming and 21st century drying. *Climate Dynamics*, 43, 2607–2627. https://doi.org/10.1007/s00382-014-2075-y.

Dai, A. (2011) Characteristics and trends in various forms of the Palmer drought severity index during 1900–2008. *Journal of Geophysical Research: Atmospheres*, 116, D12115. https://doi.org/10.1029/2010jd015541.

Dai, A. (2013) Increasing drought under global warming in observations and models. *Nature Climate Change*, 3, 52–58. https://doi.org/10.1038/nclimate1633.

Dai, A. and Wigley, T.M.L. (2000) Global patterns of ENSO-induced precipitation. *Geophysical Research Letters*, 27, 1283–1286. https://doi.org/10.1029/1999GL011140.

Donat, M.G., Lowry, A.L., Alexander, L.V., O'Gorman, P.A. and Maher, N. (2016) More extreme precipitation in the world's dry and wet regions. *Nature Climate Change*, 6, 508–513. https://doi.org/10.1038/nclimate2941.

Feng, H. and Zhang, M. (2016) Global land moisture trends: drier in dry and wetter in wet over land. *Scientific Reports*, 5, 18018. https://doi.org/10.1038/srep18018.

Global Soil Data Task Group. (2000) *Global gridded surfaces of selected soil characteristics (IGBP-DIS)*. Tennessee, Nashville: ORNL Distributed Active Archive Center. https://doi.org/10.3334/ornldaac/569.

Harris, I., Jones, P.D., Osborn, T.J. and Lister, D.H. (2014) Updated high-resolution grids of monthly climatic observations – the CRU TS3.10 dataset. *International Journal of Climatology*, 34, 623–642. https://doi.org/10.1002/joc.3711.

Held, I.M. and Soden, B.J. (2006) Robust responses of the hydrological cycle to global warming. *Journal of Climate*, 19, 5686–5699. https://doi.org/10.1175/JCLI3990.1.

Impens, I. and Lemeur, R. (1969) Extinction of net radiation in different crop canopies. *Theoretical and Applied Climatology*, 17, 403–412. https://doi.org/10.1007/bf02243377.

Kelliher, F.M., Leuning, R., Raupach, M.R. and Schulze, E.D. (1995) Maximum conductances for evaporation from global vegetation types. *Agricultural and Forest Meteorology*, 73, 1–16. https://doi.org/10.1016/0168-1923(94)02178-M.

L'Heureux, M.L., Takahashi, K., Watkins, A. B., Barnston, A. G., Becker, E. J., Di Liberto, T. E., Gamble, F., Gottschalck, J., Halpert, M. S., Huang, B., Mosquera-Vásquez, K. and Wittenberg, A. T. (2017) Observing and predicting the 2015/16 El Niño. *Bulletin of the American Meteorological Society*, 98, 1363–1382. https://doi.org/10.1175/bams-d-16-0009.1.

Li, M. and Ma, Z. (2015) Soil moisture drought detection and multitemporal variability across China. *Science China Earth Sciences*, 58, 1798–1813. https://doi.org/10.1007/s11430-015-5076-8.

Longobardi, A. and Villani, P. (2010) Trend analysis of annual and seasonal rainfall time series in the Mediterranean area. *International Journal of Climatology*, 30, 1538–1546. https://doi.org/10.1002/joc.2001.

Lu, E., Liu, S., Luo, Y., Zhao, W., Li, H., Chen, H., Zeng, Y., Liu, P., Wang, X., Wayne Higgins, R. and Halpert, M. S. (2014) The atmospheric anomalies associated with the drought over the Yangtze River basin during spring 2011. *Journal of Geophysical Research: Atmospheres*, 119, 5881–5894. https://doi.org/10.1002/2014JD021558.

Ma, F., Ye, A., You, J. and Duan, Q. (2018) 2015–16 floods and droughts in China, and its response to the strong El Niño. *Science of the Total Environment*, 627, 1473–1484. https://doi.org/10.1016/j.scitotenv.2018.01.280.

Monteith, J.L. (1965) Evaporation and the environment. *Symposia of the Society for Experimental Biology*, 19, 205–234.

Monteith, J.L. and Unsworth, M.H. (1990) *Principles of Environmental Physics*. London: Edward Asner Publishers.

Mudelsee, M. (2019) Trend analysis of climate time series: a review of methods. *Earth-Science Reviews*, 190, 310–322. https://doi.org/10.1016/j.earscirev.2018.12.005.

Ouyang, R., Liu, W., Fu, G., Liu, C., Hu, L. and Wang, H. (2014) Linkages between ENSO/PDO signals and precipitation, streamflow in China during the last 100 years. *Hydrology and Earth System Sciences*, 18, 3651–3661. https://doi.org/10.5194/hess-18-3651-2014.

Palmer, W. C. (1965) *Meteorological drought, U.S. Weather Bureau Research Paper 45*, pp. 58.

Piao, S., Ciais, P., Huang, Y., Shen, Z., Peng, S., Li, J., Zhou, L., Liu, H., Ma, Y., Ding, Y., Friedlingstein, P., Liu, C., Tan, K., Yu, Y., Zhang, T. and Fang, J. (2010) The impacts of climate change on water resources and agriculture in China. *Nature*, 467, 43–51. https://doi.org/10.1038/nature09364.

Poulter, B., Frank, D., Ciais, P., Myneni, R. B., Andela, N., Bi, J., Broquet, G., Canadell, J. G., Chevallier, F., Liu, Y. Y., Running, S. W., Sitch, S. and van der Werf, G. R. (2014) Contribution of semi-arid ecosystems to interannual variability of the global carbon cycle. *Nature*, 509, 600–603. https://doi.org/10.1038/nature13376.

Priestley, C.H. and Taylor, R.J. (1972) Assessment of surface heat-flux and evaporation using large-scale parameters. *Monthly Weather Review*, 100, 81–92.

Shao, D., Chen, S., Tan, X. and Gu, W. (2018) Drought characteristics over China during 1980–2015. *International Journal of Climatology*, 38, 3532–3545. https://doi.org/10.1002/joc.5515.

Sheffield, J., Wood, E.F. and Roderick, M.L. (2012) Little change in global drought over the past 60 years. *Nature*, 491, 435–438. https://doi.org/10.1038/nature11575.

Sun, C. and Yang, S. (2012) Persistent severe drought in southern China during winter–spring 2011: large-scale circulation patterns and possible impacting factors. *Journal of Geophysical Research: Atmospheres*, 117, D10112. https://doi.org/10.1029/2012JD017500.

Sun, P., Zhang, Q., Wen, Q., Singh, V.P. and Shi, P. (2017) Multisource data-based integrated agricultural drought monitoring in the Huai River basin, China. *Journal of Geophysical Research: Atmospheres*, 122, 10,751–710,772. https://doi.org/10.1002/2017JD027186.

Thornthwaite, C.W. (1948) An approach toward a rational classification of climate. *Geographical Review*, 38, 55–94.

Touma, D., Ashfaq, M., Nayak, M.A., Kao, S.-C. and Diffenbaugh, N.S. (2015) A multi-model and multi-index evaluation of drought characteristics in the 21st century. *Journal of Hydrology*, 526, 196–207. https://doi.org/10.1016/j.jhydrol.2014.12.011.

Trenberth, K.E., Dai, A., van der Schrier, G., Jones, P.D., Barichivich, J., Briffa, K.R. and Sheffield, J. (2014) Global warming and changes in drought. *Nature Climate Change*, 4, 17–22. https://doi.org/10.1038/nclimate2067.

van der Schrier, G., Barichivich, J., Briffa, K.R. and Jones, P.D. (2013) A scPDSI-based global data set of dry and wet spells for

1901–2009. *Journal of Geophysical Research – Atmospheres*, 118, 4025–4048. https://doi.org/10.1002/jgrd.50355.

van der Schrier, G., Jones, P.D. and Briffa, K.R. (2011) The sensitivity of the PDSI to the Thornthwaite and penman-Monteith parameterizations for potential evapotranspiration. *Journal of Geophysical Research: Atmospheres*, 116, D03106. https://doi.org/10.1029/2010jd015001.

Vicente-Serrano, S.M., Beguería, S. and López-Moreno, J.-I. (2010) A multi-scalar drought index sensitive to global warming: the standardized precipitation evapotranspiration index - SPEI. *Journal of Climate*, 23, 1696–1718.

Vicente-Serrano, S.M., Van der Schrier, G., Beguería, S., Azorin-Molina, C. and Lopez-Moreno, J.-I. (2015) Contribution of precipitation and reference evapotranspiration to drought indices under different climates. *Journal of Hydrology*, 526, 42–54. https://doi.org/10.1016/j.jhydrol.2014.11.025.

Wang, S., Huang, J., He, Y. and Guan, Y. (2014) Combined effects of the Pacific decadal oscillation and El Niño-southern oscillation on global land dry–wet changes. *Scientific Reports*, 4, 6651. https://doi.org/10.1038/srep06651.

Wang, S., Yuan, X. and Li, Y. (2017) Does a strong El Niño imply a higher predictability of extreme drought? *Scientific Reports*, 7, 40741. https://doi.org/10.1038/srep40741.

Wells, N., Goddard, S. and Hayes, M.J. (2004) A self-calibrating Palmer drought severity index. *Journal of Climate*, 17, 2335–2351. https://doi.org/10.1175/1520-0442(2004)017<2335:ASPDSI>2.0.CO;2.

Wu, J., Zha, J., Zhao, D. and Yang, Q. (2017) Changes in terrestrial near-surface wind speed and their possible causes: an overview. *Climate Dynamics*, 51, 2039–2078. https://doi.org/10.1007/s00382-017-3997-y.

Xu, K., Yang, D., Yang, H., Li, Z., Qin, Y. and Shen, Y. (2014) Spatio-temporal variation of drought in China during 1961–2012: a climatic perspective. *Journal of Hydrology*, 526, 253–264. https://doi.org/10.1016/j.jhydrol.2014.09.047.

Yan, H., Wang, S.Q., Billesbach, D., Oechel, W., Zhang, J.H., Meyers, T., Martin, T.A., Matamala, R., Baldocchi, D., Bohrer, G., Dragoni, D. and Scott, R. (2012) Global estimation of evapotranspiration using a leaf area index-based surface energy and water balance model. *Remote Sensing of Environment*, 124, 581–595. https://doi.org/10.1016/j.rse.2012.06.004.

Yan, H., Wang, S.-Q., Lu, H.-Q., Guo, A., Zhu, Z.-C., Myneni, R.B. and Shugart, H.H. (2016) Assessing spatiotemporal variation of drought in China and its impact on agriculture during 1982–2011 by using PDSI indices and agriculture drought survey data. *Journal of Geophysical Research: Atmospheres*, 121, 2283–2298. https://doi.org/10.1002/2015JD024285.

Yan, H., Wang, S.-Q., Lu, H.-Q., Yu, Q., Zhu, Z.-C., Myneni, R.B., Liu, Q. and Shugart, H.H. (2014) Development of a remotely sensing seasonal vegetation-based Palmer drought severity index and its application of global drought monitoring over 1982–2011. *Journal of Geophysical Research: Atmospheres*, 119, 2014JD021673. https://doi.org/10.1002/2014jd021673.

Yang, X., Zhao, C., Zhou, L., Wang, Y. and Liu, X. (2016) Distinct impact of different types of aerosols on surface solar radiation in China. *Journal of Geophysical Research: Atmospheres*, 121, 6459–6471. https://doi.org/10.1002/2016JD024938.

Yu, M., Li, Q., Hayes, M.J., Svoboda, M.D. and Heim, R.R. (2014) Are droughts becoming more frequent or severe in China based on the standardized precipitation evapotranspiration index:

1951–2010? *International Journal of Climatology*, 34, 545–558. https://doi.org/10.1002/joc.3701.

Zhai, P., Yu, R., Guo, Y., Li, Q., Ren, X., Wang, Y., Xu, W., Liu, Y. and Ding, Y. (2016) The strong El Niño of 2015/16 and its dominant impacts on global and China's climate. *Journal of Meteorological Research*, 30, 283–297. https://doi.org/10.1007/s13351-016-6101-3.

Zhang, R., Sumi, A. and Kimoto, M. (1999) A diagnostic study of the impact of El Niño on the precipitation in China. *Advances in Atmospheric Sciences*, 16(2), 229–241. https://doi.org/10.1007/BF02973084.

Zhang, Y., Wu, M., Li, D., Liu, Y. and Li, S. (2017) Spatiotemporal decompositions of summer drought in China and its teleconnection with Global Sea surface temperatures during 1901–2012. *Journal of Climate*, 30, 6391–6412. https://doi.org/10.1175/JCLI-D-16-0405.1.

Zhu, Z., Bi, J., Pan, Y., Ganguly, S., Anav, A., Xu, L., Samanta, A., Piao, S., Nemani, R. R. and Myneni, R. B. (2013) Global data sets of vegetation leaf area index (LAI)3g and fraction of photosynthetically active radiation (FPAR)3g derived from global inventory modeling and mapping studies (GIMMS) normalized difference vegetation index (NDVI3g) for the period 1981 to 2011. *Remote Sensing*, 5, 927–948. https://doi.org/10.3390/rs5020927.

Zou, X.K. and Zhai, P.M. (2004) Relationship between vegetation coverage and spring dust storms over Northern China. *Journal of Geophysical Research: Atmospheres*, 109, D03104. https://doi.org/10.1029/2003JD003913.

APPENDIX: | SELF-CALIBRATING PDSI$_{ARTS}$ MODEL

The PDSI$_{ARTS}$ model (Yan *et al.*, 2014) has been developed by incorporating the self-calibrating PDSI model (Wells *et al.*, 2004) with the ARTS E_0 module and snow-melting module—to account for the effects of calibration coefficients, seasonal vegetation, and snow melting.

Self-calibrating PDSI model

The original self-calibrating PDSI model (Wells *et al.*, 2004) has been adopted for global drought monitoring (Dai, 2011; van der Schrier *et al.*, 2011; Yan *et al.*, 2014), because it makes drought comparisons consistently between different climatological regions (Wells *et al.*, 2004). It computes

four values related to the soil moisture on a monthly scale by using a two-layer soil water balance model driven by precipitation (P_r) and potential evapotranspiraiton (E_p). The four values are evapotranspiraiton (E), recharge to soil layers (R), runoff (O), and water loss from soil layers (L).

The PDSI model is sensitive to the driving forcing of potential evaporation (E_P) or reference evaporation (E_0). Because Penman-Monteith E_{P_PM} model (Monteith, 1965) accounts for the radiative and aerodynamic processes (Sheffield *et al.*, 2012), the E_{P_PM} has been suggested as appropriate to drive the self-calibrating PDSI model. However E_{P_PM} typically calculates surface conductance directly from L_{ai} with an assumption of "big leaf" canopy and neglects soil evaporation. To solve this problem, the self-calibrating PDSI$_{ARTS}$ model adopts the ARTS E_0 module (Yan *et al.*, 2012) that calculates plant transpiration (E_c) and soil evaporation (E_s) separately.

ARTS E_0 module

As a canopy conductance-based two-source E_0 model with an assumption of adequate soil water availability, the ARTS E_0 module (Yan *et al.*, 2012) calculates plant transpiration (E_c) and soil evaporation (E_s), respectively,

$$E_0 = E_c + E_s \tag{A1}$$

The net radiation (R_n) is partitioned to a soil part (R_{ns}; Impens and Lemeur (1969)) and a canopy part (R_{nc}),

$$R_{ns} = R_n \exp(-k_A L_{ai}) \tag{A2}$$

$$R_{nc} = R_n - R_{ns} \tag{A3}$$

where R_{nc} and R_{ns} are parts of the net radiation that are absorbed by the canopy and the soil, respectively, and k_A equals 0.6 (Impens and Lemeur, 1969; Chen *et al.*, 1997).

The canopy transpiration (E_c) model is calculated from a modified Penman-Monteith model with input of the canopy-absorbed net radiation R_{nc} and canopy conductance (G_c),

$$E_c = \frac{\Delta R_{nc} + \rho C_p D G_a}{\Delta + \gamma(1 + G_a/G_c)} \tag{A4}$$

$$G_c = g_{smax} \times R_h \times L_{ai} \tag{A5}$$

where R_{nc} is the net radiation absorbed by the canopy; Δ is the gradient of the saturated vapour pressure to air

temperature; γ is the psychrometric constant; ρ is the density of air; C_p is the specific heat of air at constant pressure; G_a is the aerodynamic conductance accounting for wind speed impact (Monteith and Unsworth, 1990); G_c is the canopy conductance accounting for transpiration from the vegetation; and D equals $e_s - e_a$ and is the vapour pressure deficit of the air, with e_s is the saturation water vapour pressure at air temperature and e_a is the actual water vapour pressure, R_h is the relative humidity, and g_{smax} is the maximum stomatal conductance assumed to have a value of 12.2 mm s^{-1} (Kelliher *et al.*, 1995). L_{ai} is the leaf area index used for scaling stomatal conductance to canopy conductance for a large-scale application of the Penman-Monteith equation.

The soil evaporation (E_s) equation is modified from an air-relative-humidity-based evapotranspiration model,

$$E_s = 1.35 R_h \frac{\Delta R_{ns}}{\Delta + \gamma} \tag{A6}$$

which scales the Priestley and Taylor (1972) equilibrium evaporation to wet surface E_s by using R_h as a complementary relationship coefficient with an assumption of adequate soil water availability.

Snow-melting and accumulation module

The PDSI$_{ARTS}$ model adopts a snow-melting and accumulation module to account for the effect of snow melting (Yan *et al.*, 2012). The water supply P, defined as the sum of precipitation and snowmelt, is used to substitute for the more usual P_r to drive the self-calibrating PDSI$_{ARTS}$ model on a monthly scale.

With a temperature threshold of 0°C, precipitation P_r is divided into precipitation and snowfall; snowfall is then added to the snowpack (S_{now}). Snowmelt is calculated from snowpack using a simple temperature-based snowmelt function (S_f).

$$P = P_r + S_{now} \times S_f \tag{A7}$$

$$S_f = \begin{cases} 0 & \text{if } T_a \leq 0°C \\ 0.2 T_a & \text{if } 0°C < T_a \leq 5°C \\ 1 & \text{if } T_a > 5°C \end{cases} \tag{A8}$$

where P is the water input (mm month^{-1}) including precipitation (P_r) and snowmelt, S_f is the snow melting factor, T_a is the air temperature (°C).